Mathematical Biosciences and Engineering

http://www.aimspress.com/journal/mbe

MBE, 20(10): 18774–18791.
DOI: 10.3934/mbe.2023832
Received: 05 August 2023
Revised: 29 August 2023
Accepted: 24 September 2023
Published: 09 October 2023

Research article

Adaptive nonsingular terminal sliding mode controller for PMSM drive system using modified extended state observer

Ying Shi[1,*] **and Keqi Mei**[2]

[1] School of Electronic and Optical Engineering, Nanjing University of Science and Technology Zijin College, Nanjing 210023, China

[2] School of Electrical and Information Engineering, Jiangsu University, Zhenjiang 212013, China

* **Correspondence:** Email: shiyingzj@hotmail.com.

Abstract: In this study, a novel adaptive nonsingular terminal sliding mode (ANTSM) control frame combined with a modified extended state observer (MESO) is presented to enhance the anti-interference performance of the permanent magnet synchronous motor (PMSM) system. In the face of time-varying disturbances with unknown upper bounds, traditional nonsingular terminal sliding mode (NTSM) controllers typically utilize the large control gain to counteract the total disturbance, which will cause unsatisfactory control performances. To address this tough issue, an ANTSM control technique was constructed for the PMSM system by tuning the control gain automatically without overestimation. On this basis, the MESO was adopted to estimate the unknown total disturbance, whose estimation was offset to the ANTSM control input. By applying finite-time techniques, the estimation error will finite-time converge to zero. The proposed MESO has a more rapid estimation speed than the traditional extended state observer (ESO). Finally, the validity of the ANTSM + ESO composite control algorithm is confirmed by comprehensive experiments.

Keywords: PMSM; disturbance observer; terminal sliding mode; composite control; adaptive law

1. Introduction

Owing to the distinctive characteristics of high power density and high efficiency, permanent magnet synchronous motor (PMSM) has drawn extensive popularity over the last several decades [1–3]. For this reason, PMSM has been widely applied for industry, especially for electric vehicles, vacuum cleaners, electric ship propulsion and more. Nevertheless, the traditional proportional integral (PI) control algorithm is typically difficult to offer the high-precision control property [4–7]. To improve the unsatisfactory performance of the PI controller, lots of advanced algorithms have been applied to further optimize the control precision, such as predictive control [8,9], fuzzy control [10–13], adaptive

control [14–18] and sliding mode control (SMC) [19–23].

Among the previously mentioned modern control approaches, the SMC is an effective strategy to enhance the anti-disturbance capability of the PMSM system [24]. A traditional linear SMC method was presented in [25] to obtain a fast dynamic response and strong robustness. However, the parameter variation has not been completely considered in theory, which limits the stable operation of motors. In [26], a new piecewise but differentiable switching controller was introduced with a proper design idea to avert the singularity problem. Moreover, in order to make the speed error converge faster, the nonsingular terminal sliding mode (NTSM) control algorithm was proposed [27] to make sure that the speed error will finite-time converge to the origin.

The NTSM strategy can handle the singular issue and provide satisfactory tracking accuracy. However, the NTSM controller still brings severe chattering [28, 29], and a fast NTSM controller with no switching function was used to weaken the chattering [30]. However, this kind of controller has poor anti-disturbance performance and only converges the speed error to a region instead of to zero. At the same time, a brand-new adaptive terminal sliding mode (TSM) reaching law combined with a fast TSM control method was utilized to construct the speed controller for the PMSM system in [31]. Even if an adaptive law was adopted to reduce chattering, this method still cannot adjust the control gain automatically with the change of total disturbance.

Notably, utilizing the disturbance observer (DOB) to estimate the unknown time-varying disturbance is a valid strategy to avoid the overestimated switching gain in SMC [32–34]. Compensating the precise estimates to the baseline controller, the PMSM drive system will achieve significant steady-state performance and strong disturbance rejection property synchronously [35]. Without the accurate information of the PMSM mathematical model, a conventional extended state observer (ESO) was applied [36] to restrain the property deterioration of PMSM in the existence of external disturbance and parameter variation. Unfortunately, the baseline controller only adopted the linear PI method. It is extremely hard for this category of composite controllers to achieve strong disturbance rejection property. On this basis, the traditional ESO combined with a simple SMC algorithm was constructed [37] to address the above tough issue. Although the traditional ESO can estimate the total disturbance exactly, it just guarantees that the estimated error converges asymptotically to zero, which may result in poor estimation precision. In order to obtain higher estimation accuracy and robustness, various improved ESOs have been proposed in recent years [38, 39]. In [40], the natural evolution theory has been applied to graph structure learning, where an evolutionary method was constructed to evolve a population of graph neural network (GNN) models to adapt to dynamical environments. In [41], a heterogeneous network representation learning method was reported to characterize implicitly inside Ethereum transactions. In [42], a center-based transfer feature learning with classifier adaptation for the surface defect recognition was proposed. In [43], the authors proposed an integrated triboelectric nanogenerator and tribovoltaic nanogenerator in the air cylinder as difunctional pneumatic sensors for simultaneous position and velocity monitoring. In [44], the recent developments in the area of arc fault detection were studied.

In this paper, a novel adaptive nonsingular terminal sliding mode (ANTSM) controller combined with a modified ESO (MESO) is proposed to enhance the disturbance rejection property of the PMSM system. First of all, considering the parameter variation and time-varying load torque, an ANTSM controller is constructed to provide the desired steady-state and dynamic performance. Furthermore, in order to solve the trouble of unsatisfactory control effect due to large switching gain, one novel

MESO is utilized to observe the unknown time-varying disturbance and compensate the estimates to the ANTSM controller simultaneously. Lastly, the validity of the ANTSM + ESO composite control algorithm is proved by comprehensive experiments. The main contribution of this article could be summarized in the following points:

1) A novel NTSM controller is designed. The control gain is automatically tuned by the proposed adaptive law. It avoids unsatisfactory control performance caused by excessive control gain.
2) A MESO is proposed to improve the anti-disturbance capability of the PMSM system. By using the finite-time technique, the estimation error can converge to zero in finite time. The proposed MESO has a higher estimation accuracy and faster estimation speed.
3) The proposed composite controller combines the ANTSM algorithm with MESO to improve the system robustness. Since the high disturbance estimation accuracy of MESO, the rejection ability to disturbances of the PMSM speed regulation system can be improved.

The rest of the paper is organized as follows. In Section 2, the PMSM mathematical model with parameter perturbation and the traditional NTSM control method are described. Section 3 shows the design of the proposed MESO-based ANTSM controller in detail. Comprehensive experiments are illustrated in Section 4. The summary of this paper is presented in Section 5.

Notations: Throughout the paper, the symbol $\lfloor x \rceil^m$ is used to present the $|x|^m \cdot \text{sign}(x)$ for a real number m, and the symbol $\lfloor x \rceil^*$ is defined as

$$\lfloor x \rceil^* = \begin{cases} 1, x \geq 0 \\ 0, x < 0 \end{cases}.$$

2. Problem formulation

2.1. Mathematical model of PMSM

In the ideal case, the motion equation of PMSM can be given by

$$\dot{\Omega}=\frac{1.5 n_p \psi_f}{J} i_q - \frac{B}{J}\Omega - \frac{T_L}{J} \tag{2.1}$$

where Ω is the rotor angular speed, n_p is the number of pole pairs, ψ_f is the flux linkage, J is the moment of inertia, B is the viscous friction coefficient, i_q is the stator current in the q-axis and T_L is the load torque.

Because of load variation in practical applications, the value of inertia may be mismatched. Therefore, we introduce $\Delta J = J - J_0$, where J_0 is the nominal value and ΔJ is parameter variation. Then, replacing current i_q by the reference current i_q^*, system (1) can be rewritten as

$$\begin{aligned} \dot{\Omega} &= \frac{1.5 n_p \psi_f}{J_0} i_q - \frac{B}{J_0}\Omega + d_0(t) \\ &= b i_q^* - \frac{B}{J_0}\Omega + d_0(t) \end{aligned} \tag{2.2}$$

where $d_0(t) = -\frac{T_L}{J_0} + b\left(i_q - i_q^*\right) - \frac{\Delta J}{J_0}\dot{\Omega}$ and $b = \frac{1.5 n_p \psi_f}{J_0}$.

2.2. Traditional NTSM controller design

The traditional NTSM algorithm is used to design the speed controller for the PMSM system in this subsection. First of all, setting Ω_r as the reference speed, the speed error Ω_e is expressed as

$$\Omega_e = \Omega_r - \Omega. \tag{2.3}$$

With the help of (2.2), one has

$$\dot{\Omega}_e = -bi_q^* - \frac{B}{J_0}\Omega_e + d(t) \tag{2.4}$$

where $d(t) = -d_0(t) + \dot{\Omega}_r + \frac{B}{J_0}\Omega_r$ is the total disturbance.

Assumption 1: [45–47] *The total disturbance $d(t)$ is bounded and differentiable, and there exist known positive constants l_1 and l_2 such that $|d(t)| \le l_1$ and $|\dot{d}(t)| \le l_2$.*

Remark 1: From (2.2) and (2.4), we can get that the disturbance $d(t)$ consists of the load torque T_L, the stator current i_q, the stator reference current i_q^*, the speed Ω, the setting speed Ω_r and other components. It can be concluded that the above variables are bounded and differentiable. Therefore, it is reasonable that the total disturbance satisfies $|d(t)| \le l_1$ and $|\dot{d}(t)| \le l_2$, where l_1 and l_2 are known positive constants.

According to [48], the nonsingular terminal sliding manifold is selected as

$$s = \int \Omega_e \, dt + \frac{1}{\beta}\Omega_e^{p/q} \tag{2.5}$$

where β is positive constant, p and q are positive odd integers and $1 < p/q < 2$.

Based on this, the NTSM controller will be designed as

$$i_q^* = \frac{1}{b}\left(-\frac{B}{J_0}\Omega_e + \beta\frac{q}{p}\Omega_e^{2-p/q} + k \cdot \operatorname{sign}(s)\right) \tag{2.6}$$

with a positive constant k.

Choose the widely-used Lyapunov function as

$$V(s) = \frac{1}{2}s^2. \tag{2.7}$$

Differentiating $V(s)$ gets

$$\begin{aligned} \dot{V}(s) &= s\dot{s} \\ &= s\left(\Omega_e + \frac{p}{\beta q}\Omega_e^{p/q-1}\dot{\Omega}_e\right) \\ &= s\frac{p}{\beta q}\Omega_e^{p/q-1}\left(-bi_q^* - \frac{B}{J_0}\Omega_e + d(t) + \beta\frac{q}{p}\Omega_e^{2-p/q}\right). \end{aligned} \tag{2.8}$$

Substituting NTSM controller (2.6) into (2.8), one obtains

$$\dot{V}(s) = s\frac{p}{\beta q}\Omega_e^{p/q-1}(-k \cdot \operatorname{sign}(s) + d(t))$$

$$\leq -\frac{p}{\beta q}\Omega_e^{p/q-1}|s|k + \frac{p}{\beta q}x^{p/q-1}|s||d(t)|$$
$$\leq -\frac{p}{\beta q}\Omega_e^{p/q-1}|s|\left(k - l_1\right). \tag{2.9}$$

Similar to [27], if the control gain satisfies $k > l_1$, then the speed error will converge to origin in a finite time.

Remark 2: To guarantee the stability of the PMSM, the value of k in the traditional NTSM controller should be chosen to be larger than the upper bound of the total disturbance. However, the total disturbance in practical engineering is time-varying, and its upper bound may be much smaller than the fixed control gain. Since the control gain directly affects the chattering amplitude, conservative control gain may lead to unsatisfactory control performance in PMSM. Thus, it is urgent to design a novel controller with variable and a small enough control gain to suppress the time-varying disturbance.

3. Proposed controller design

To address the forgoing disadvantages of the conventional NTSM controller, a novel ANTSM is developed in this section to automatically tune the value of control gains. Based upon this, compensating the disturbance estimation value derived by MESO to the ANTSM controller, the control gain can get a further reduction.

3.1. Construction of ANTSM controller

With the aid of controller (2.6), the ANTSM controller is constructed as

$$i_q^* = \frac{1}{b}\left(-\frac{B}{J_0}\Omega_e + \beta\frac{q}{p}\Omega_e^{2-p/q} + k\left(t\right)\cdot \operatorname{sign}\left(s\right)\right). \tag{3.1}$$

The adaptive law $k(t)$ is given as

$$\begin{cases} \dot{k}(t) = \eta\cdot k(t)\cdot \operatorname{sign}(\delta(t)) + N[k_M - k(t)]^* \\ \qquad\quad + N[k_m - k(t)]^* \\ \delta(t) = |[\operatorname{sign}(s)]_{av}| - \varepsilon, \end{cases} \tag{3.2}$$

where $k_M > l_1$ and $k_m > 0$ are the maximums and minimums of the control gain, constant $\varepsilon \in (0, 1)$, $\eta > \frac{l_2}{\varepsilon k_m}$, $N > \eta k_M$, and $[\operatorname{sign}(s)]_{av}$ is produced by the signal $z(t)$ of the low-pass filter

$$\dot{z} = \frac{1}{\lambda}\left(\operatorname{sign}\left(\mathrm{s}\right) - z\right), \quad z\left(0\right) = 0 \tag{3.3}$$

with λ being the tunable parameter. The ANTSM controller structure is depicted by Figure 1.

Remark 3: Since the discontinuous switching function $\operatorname{sign}(s)$ varies at negative one and one, the function $[\operatorname{sign}(s)]_{av}$ is continuous and its value belongs to $(-1, 1)$. Therefore, it can be assumed that the second derivative of function $[\operatorname{sign}(s)]_{av}$ satisfies $|\frac{d^2}{dt^2}[\operatorname{sign}(s)]_{av}| \leq C$ and $C > 0$.

Next, we will prove that $k(t)$ can converge in a finite time to the minimum absolute value of the total uncertainty. In addition, the equivalent control theory is crucial for the proof in the paper.

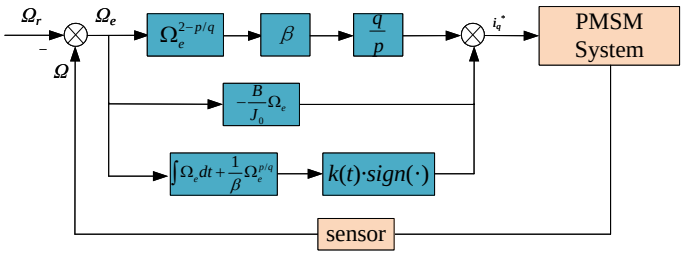

Figure 1. The diagram of proposed ANTSM controller.

The equivalent controller is constructed as

$$u_{eq} = \frac{1}{b}\left(-\frac{B}{J_0}\Omega_e + \beta\frac{q}{p}\Omega_e^{2-p/q} + d(t)\right). \tag{3.4}$$

Since the exact information about the total disturbance $d(t)$ is not available, the equivalent controller (3.4) cannot be directly applied to the PMSM system. Therefore, an average control of ANTSM controller (3.1) is employed to track controller (3.4). Meanwhile, to enhance the accuracy of the average control, a continuous function $[\text{sign}(s)]_{av}$ is used to replace the discontinuous function $\text{sign}(s)$ in equivalent controller. Then, the average control of ANTSM controller (3.1) is constructed as

$$u_{av} = \frac{1}{b}\left(-\frac{B}{J_0}\Omega_e + \beta\frac{q}{p}\Omega_e^{2-p/q} + k\,(t)\cdot[\text{sign}\,(s)]_{av}\right). \tag{3.5}$$

According to the above analysis, if the average control (3.5) can track the equivalent controller (3.4) well, one has

$$d(t) = k(t)\cdot[\text{sign}(s)]_{av}. \tag{3.6}$$

If $[\text{sign}(s)]_{av}$ approaches one, the $k(t)$ is sufficiently large to counteract the $d(t)$. The basic idea of the ANTSM control approach is to ensure that $k(t)$ can converge to $\frac{|d(t)|}{|[\text{sign}(s)]_{av}|}$ with ε being close to one in a finite time. Meanwhile, the continuous function $[\text{sign}(s)]_{av}$ should converge to parameter ε.

Consider the following Lyapunov function:

$$V_1(\delta) = \frac{1}{2}\delta^2. \tag{3.7}$$

Evaluating the derivative of $V_1(\delta)$ yields

$$\dot{V}_1(\delta) = \delta\dot{\delta} = \delta\frac{d}{dt}\left(\frac{|d\,(t)|}{k\,(t)}\right). \tag{3.8}$$

Since the range of control gain $k\,(t) \in [k_m, k_M]$, one has $\frac{|d(t)|}{\varepsilon} > k_m$. With the help of Assumption 1, (3.8) can be rewritten as

$$\dot{V}_1(\delta) \le -|\delta|k^{-1}(t)(\varepsilon k_m\eta - l_2). \tag{3.9}$$

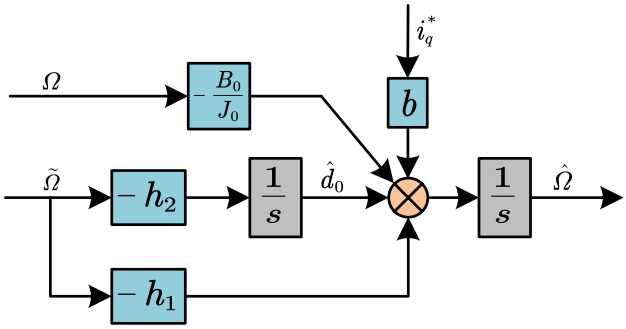

Figure 2. Diagram of traditional ESO.

Combining $\eta > \frac{l_2}{\varepsilon k_m}$ and (3.9), one has

$$\dot{V}_1(\delta) \leq -\frac{|\delta|(\varepsilon k_m \eta - l_2)}{k_M} = -\kappa V_1^{\frac{1}{2}}(\delta) \tag{3.10}$$

where $\kappa = \frac{\sqrt{2}(\varepsilon k_m \eta - l_2)}{k_M} > 0$.

Therefore, inequity (3.10) satisfies the finite-time stability theorem [49], and it indicates that $k(t)$ will converge to $\frac{|d(t)|}{\varepsilon}$.

3.2. Construction of MESO

In this subsection, the conventional ESO and the presented MESO are exploited to estimate the disturbance $d_0(t)$, respectively. First, provided that $|\dot{d}_0| \leq l_0, l_0 > 0$, the traditional ESO designed for system (2.2) can be expressed as

$$\begin{cases} \dot{\hat{\Omega}} = \hat{d}_0 - \frac{B}{J_0}\Omega + bi_q^* - h_1\tilde{\Omega}, \\ \dot{\hat{d}}_0 = -h_2\tilde{\Omega} \end{cases} \tag{3.11}$$

where $\tilde{\Omega} = \hat{\Omega} - \Omega$, $\hat{\Omega}$ and $\hat{d}_0$ are the estimated values of Ω and d_0, h_1 and h_2 are the gains of traditional ESO.

Nevertheless, the traditional ESO just ensures that the estimation of error converges to zero asymptotically, which causes poor estimation precision. Therefore, it is urgent to accelerate the estimation speed of traditional ESO. For (2.2), the MESO is constructed as

$$\begin{cases} \dot{\hat{\Omega}} = \hat{d}_0 - \frac{B}{J_0}\Omega + bi_q^* - h_1\phi_1\left(\tilde{\Omega}\right), \\ \dot{\hat{d}}_0 = -h_2\phi_2\left(\tilde{\Omega}\right) \end{cases} \tag{3.12}$$

where functions $\phi_1\left(\tilde{\Omega}\right)$ and $\phi_2\left(\tilde{\Omega}\right)$ are given by

$$\begin{aligned} \phi_1\left(\tilde{\Omega}\right) &= \left\lfloor \tilde{\Omega} \right\rceil^{\frac{1}{2}} + \tilde{\Omega}, \\ \phi_2\left(\tilde{\Omega}\right) &= \frac{1}{2}\mathrm{sign}\left(\tilde{\Omega}\right) + \frac{3}{2}\left\lfloor \tilde{\Omega} \right\rceil^{\frac{1}{2}} + \tilde{\Omega}. \end{aligned} \tag{3.13}$$

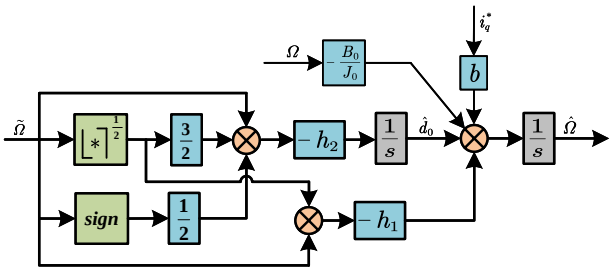

Figure 3. Diagram of proposed MESO.

Subtracting (3.12) from (2.2) obtains

$$\begin{cases} \dot{\tilde{\Omega}} = \tilde{d}_0 - h_1\phi_1\left(\tilde{\Omega}\right), \\ \dot{\tilde{d}}_0 = -h_2\phi_2\left(\tilde{\Omega}\right) - \dot{d}_0 \end{cases} \tag{3.14}$$

where $\tilde{d}_0 = \hat{d}_0 - d_0$.

By defining $\xi^T = \left[\phi_1\left(\tilde{\Omega}\right), \tilde{d}_0\right]$, the time derivative of ξ can be written as

$$\begin{aligned} \dot{\xi} &= \Phi\left(\tilde{\Omega}\right)\begin{bmatrix} -h_1\phi_1\left(\tilde{\Omega}\right) + \tilde{d}_0 \\ -h_2\phi_1\left(\tilde{\Omega}\right) - \dfrac{\dot{d}_0}{\Phi\left(\tilde{\Omega}\right)} \end{bmatrix} \\ &= \Phi\left(\tilde{\Omega}\right)(A\xi - B\psi) \end{aligned} \tag{3.15}$$

where $A = \begin{bmatrix} -h_1 & 1 \\ -h_2 & 0 \end{bmatrix}$, $B = \begin{bmatrix} 0 \\ 1 \end{bmatrix}$, $\Phi\left(\tilde{\Omega}\right) = \frac{3}{2}\left|\tilde{\Omega}\right|^{\frac{1}{2}} + 1$ and $\psi = \dot{d}_0/\Phi\left(\tilde{\Omega}\right)$.

With the help of $|\dot{d}_0| \le l_0$, one yields $|\psi| \le l_0$. Then, we define

$$\begin{aligned} \Gamma(\psi,\xi) &= \begin{bmatrix} \xi \\ \psi \end{bmatrix}^T \begin{bmatrix} l_0^2 & 0 \\ 0 & -1 \end{bmatrix}\begin{bmatrix} \xi \\ \psi \end{bmatrix} \\ &= \begin{bmatrix} \phi_1(\tilde{\Omega}) & \tilde{d}_0 & \psi \end{bmatrix}\begin{bmatrix} l_0^2 & 0 \\ 0 & -1 \end{bmatrix}\begin{bmatrix} \phi_1(\tilde{\Omega}) \\ \tilde{d}_0 \\ \psi \end{bmatrix} \\ &= \begin{bmatrix} \xi^T & \psi \end{bmatrix}\begin{bmatrix} l_0^2 & 0 \\ 0 & -1 \end{bmatrix}\begin{bmatrix} \xi \\ \psi \end{bmatrix} \\ &= -\psi^2 + l_0^2 \\ &\ge 0. \end{aligned} \tag{3.16}$$

Theorem 1: *For a positive constant γ and the symmetric and positive definite matrix Q, if the following inequality holds*

$$\begin{bmatrix} A^TQ + QA + \gamma Q + l_0^2 & QB \\ B^TQ & -1 \end{bmatrix} \le 0,$$

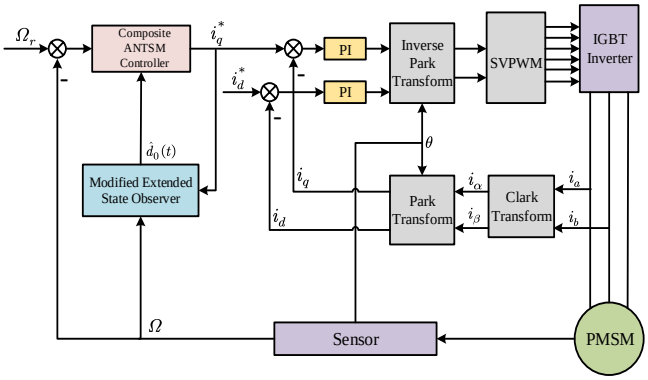

Figure 4. Control scheme of proposed ANTSM+MESO controller.

then the estimation error of the proposed MESO (3.12) *will converge to zero in a finite time.*

Proof. The Lyapunov function is chosen as

$$V_2 = \xi^T Q \xi. \tag{3.17}$$

From (3.15) and (3.16), the differential coefficient of V_2 can be given as

$$\begin{aligned}
\dot{V}_2 &= \Phi(\tilde{\Omega})\left[\xi^T\left(A^T Q + PA\right)\xi + \psi B^T Q\xi + \xi^T QB\psi\right] \\
&= \Phi(\tilde{\Omega})\begin{bmatrix} \xi \\ \psi \end{bmatrix}^T \begin{bmatrix} A^T Q + QA & QB \\ B^T Q & 0 \end{bmatrix}\begin{bmatrix} \xi \\ \psi \end{bmatrix} \\
&\le \Phi(\tilde{\Omega})\left\{\begin{bmatrix} \xi \\ \psi \end{bmatrix}^T \begin{bmatrix} A^T Q + QA & QB \\ B^T Q & 0 \end{bmatrix}\begin{bmatrix} \xi \\ \psi \end{bmatrix} + \Gamma(\psi,\xi)\right\} \\
&\le \Phi(\tilde{\Omega})\begin{bmatrix} \xi \\ \psi \end{bmatrix}^T \begin{bmatrix} -\gamma Q & 0 \\ 0 & 0 \end{bmatrix}\begin{bmatrix} \xi \\ \psi \end{bmatrix} \\
&= \Phi(\tilde{\Omega})\left(-\gamma\xi^T Q\xi\right) \\
&= -\Phi(\tilde{\Omega})\gamma V_2 \\
&= -\frac{1}{2|\tilde{\Omega}|^{\frac{1}{2}}}\gamma V_2 - \gamma V_2.
\end{aligned} \tag{3.18}$$

From (3.17), it is derived that

$$\lambda_{\min}\{Q\}\,\|\xi\|_2^2 \le \xi^T Q\xi \le \lambda_{\max}\{Q\}\,\|\xi\|_2^2 \tag{3.19}$$

where $\lambda\{\cdot\}$ is the eigenvalue of matrix $\{\cdot\}$ and $\|\xi\|_2^2$ is the Euclidean norm of ξ.

Considering $\|\xi\|_2^2 = \left|\tilde{\Omega}\right| + 2\left|\tilde{\Omega}\right|^{\frac{3}{2}} + \tilde{\Omega}^2 + \tilde{d}_0^2$, it follows that

$$\left|\tilde{\Omega}\right|^{\frac{1}{2}} \le \|\xi\|_2 \le \frac{V_2^{\frac{1}{2}}}{\lambda_{\min}^{\frac{1}{2}}\{P\}}. \tag{3.20}$$

In accordance with (3.18) and (3.20), one obtains

$$\dot{V}_2 \le -\frac{1}{2|\tilde{\Omega}|^{\frac{1}{2}}}\gamma V_2 - \gamma V_2$$

Table 1. Parameters of the PMSM.

Name	Value and unit
dc-bus voltage	220 V
Rated torque	10 $N \cdot m$
Machine pole pairs	4
Rated speed	1500 rpm
Rotor flux linkage	0.142 wb
Moment of inertia	1.94 Kg/m^2
Rated power	1.5 kW
Stator resistance	1.5 Ω
Sampling frequency	10 kHz

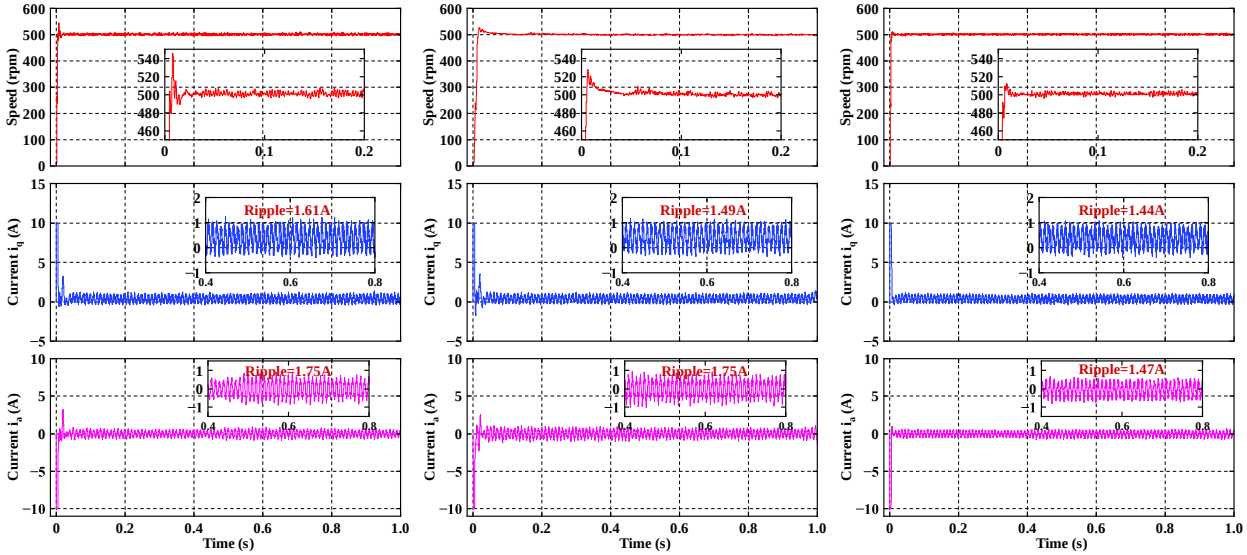

Figure 5. Response curve under the step change of speed in the start-up phase. (a) PI. (b) NTSM (c) ANTSM.

$$\leq -\frac{\gamma\lambda^{\frac{1}{2}}\min\{P\}}{2}V_2^{\frac{1}{2}} - \gamma V_2. \tag{3.21}$$

Clearly, (3.21) satisfies the finite-time stability theory [50]. To this end, we have proved that under the proposed MESO (3.12) the estimation error will be guaranteed to converge to zero in a finite time.

The proposed MESO can estimate the disturbance precisely. Then, compensating the estimate $\hat{d}_0(t)$ to the baseline controller, the output signal of the MESO-based ANTSM controller can be designed as

$$i_q^* = \frac{1}{b}\left(-\frac{B}{J_0}\Omega_e + \beta\frac{q}{p}x^{2-p/q} + k(t)\cdot\text{sign}(s) - \hat{d}_0(t)\right). \tag{3.22}$$

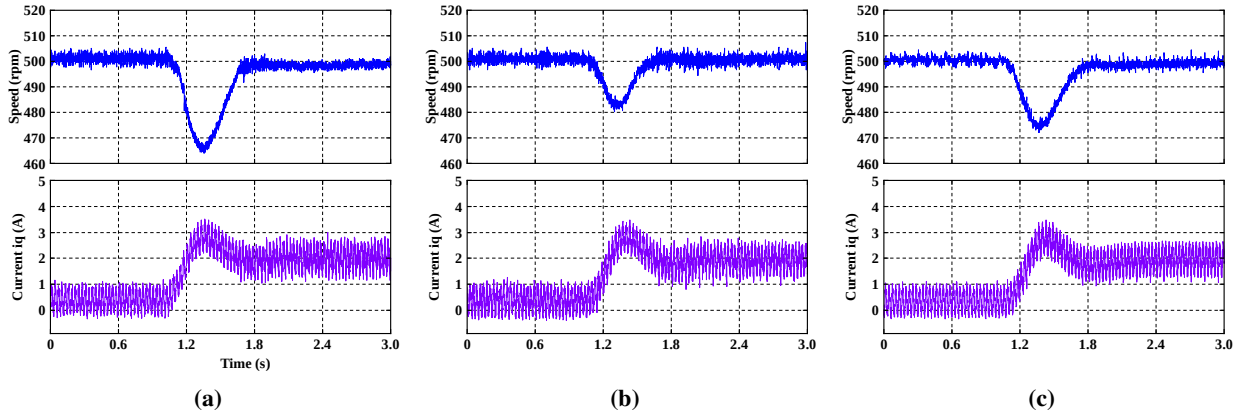

Figure 6. Response curves under a sudden load torque change. (a) PI. (b) NTSM. (c) ANTSM.

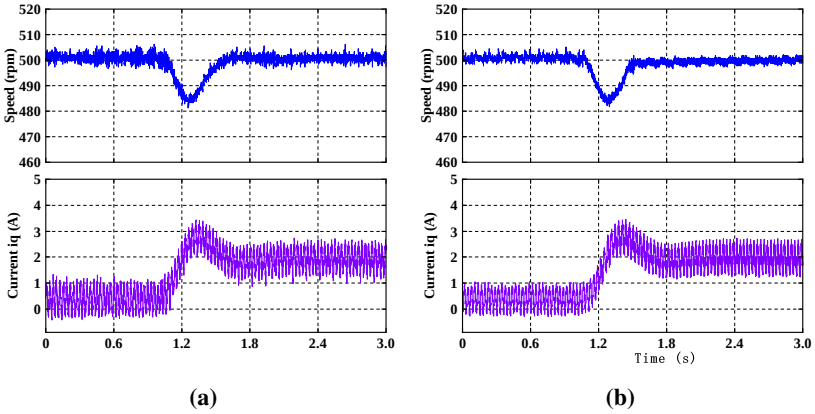

Figure 7. Response curves under a sudden load torque change. (a)ANTSM+ESO. (b) ANTSM + MESO.

4. Experimental validation

Aiming to validate the performance of the ANTSM + MESO control algorithm, comprehensive experimental results are given in this section. The complete schematic of the proposed ANTSM + MESO control system is illustrated in Figure 4. The experimental platform mainly consists of a three-phase motor, a controller, a three-phase inverter, a host computer and more. The controlled motor is a permanent magnet synchronous motor with a power of 1.5 KW, and the motor parameters are illustrated in Table 1. The controller is based on the RTU-BOX204 real-time digital control platform. The magnetic powder brake is used to generate the load torque. The parameters of the ANTSM controller are chosen as $\beta = 600$, $q = 11$, $p = 17$, $\eta = 1.5$, $\varepsilon = 0.99$, $N = 80$, $k_m = 1$ and $k_M = 30$, and the parameters of MESO are selected as $h_1 = 30$ and $h_2 = 225$.

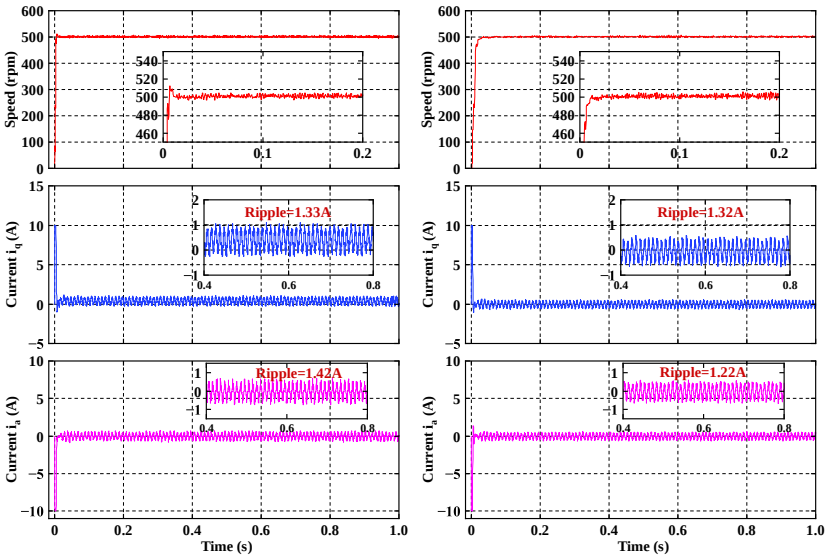

Figure 8. Response curve under the step change of speed in the start-up phase. (a)ANTSM+ESO. (b) ANTSM + MESO.

4.1. Comparison of experimental results among PI, traditional NTSM and ANTSM

The start-up results of ω, i_q and i_a under the PI, traditional NTSM and the proposed ANTSM controller are respectively depicted in Figure 5. The given speed is 500 *rpm*, and no additional load torque was added. One can notice that the start-up transient response under the PI has the longest convergence time and largest speed overshoot. In Figure 5(c), the developed ANTSM controller has the smaller start speed overshoot. Figure 6 shows a sudden load experiment. From the experimental results, one can see that the proposed ANTSM controller has the smallest speed fluctuation and current ripple.

4.2. Comparison of experimental results among ANTSM+ESO and ANTSM+MESO

In this subsection, the ESO-based ANTSM controller is utilized to compare with the presented MESO-based ANTSM controller. Figure 7 exhibits the sudden load change responses at the speed of 500 *rpm*. After loading, the speed recovery time under the proposed ANTSM+MESO controller is shorter than that under the ANTSM+ESO controller, and the speed fluctuation under the proposed ANTSM+MESO controller is also smaller. The starting responses are depicted by Figure 8. One can undoubtedly observe that the speed overshoot of the proposed ANTSM+MESO controller is smaller than that under the ANTSM+ESO. Additionally, the time for the q-axis and a-phase currents to achieve the system stability was shorter than that under the ANTSM+ESO controller.

4.3. Experimental results of dynamic performance tests

To further validate the availability of the proposed controller, numerous additional experiments were carried out. The moment of inertia has a straightforward impact on the starting and braking performance of the motor. As a result, the controller performance was tested by changing the value of

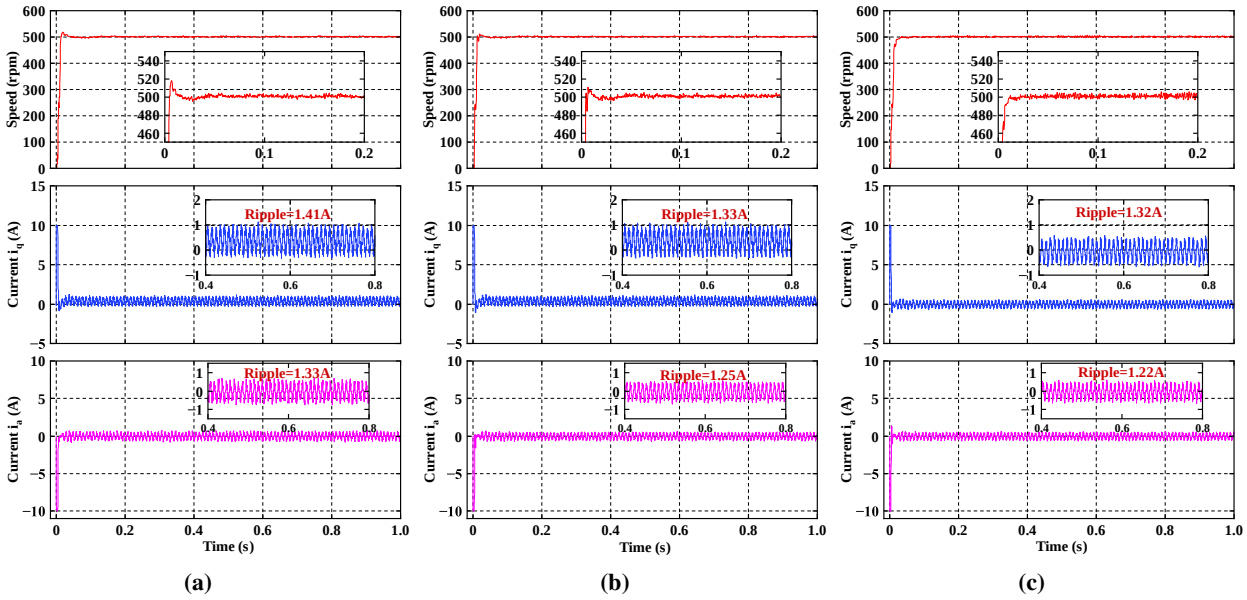

Figure 9. Step response of the ANTSM+MESO controller. (a) $J=(1/3)\,J_0$. (b) $J=(1/2)\,J_0$. (c) $J=J_0$.

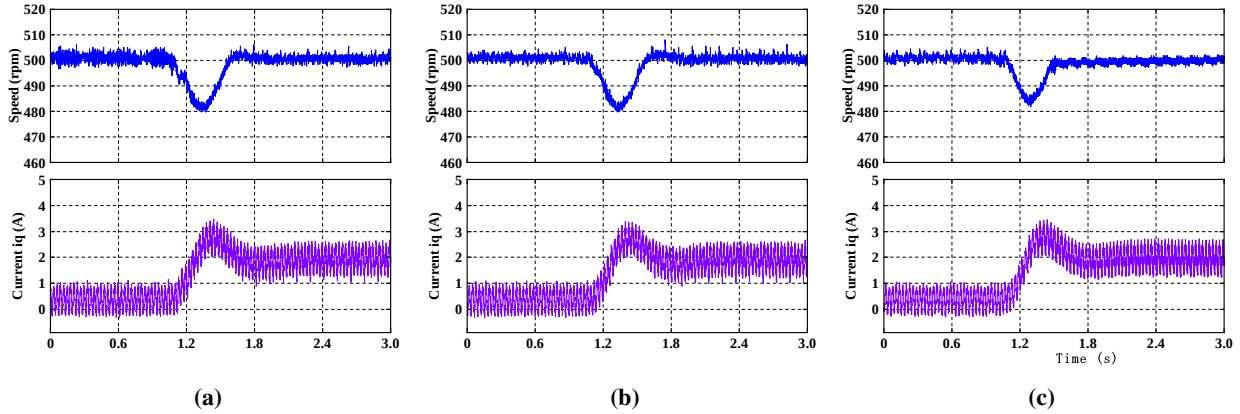

Figure 10. Speed responses of the ANTSM+MESO controller under a sudden load torque change. (a) $J=(1/3)\,J_0$. (b) $J=(1/2)\,J_0$. (c) $J=J_0$.

inertia in the presented ANTSM+MESO controller. The inertia $J=(1/3)\,J_0$, $J=(1/2)\,J_0$ and $J=J_0$ were chosen for comparative experiments. Figure 9 shows the step speed responses at the three different inertia. The sudden load change responses at the speed of 500 *rpm* are exhibited by Figure 10. As can be seen in Figures 9 and 10, the inertia mismatch imposes an impact on the stable operation of the motor. Nevertheless, the system can still operate stably under the proposed ANTSM+MESO controller.

The experimental results of speed, current i_q and current i_a during the speed change are shown in Figure 11(a). The anti-disturbance property of the ANTSM + MESO control strategy at 500 *rpm* is exhibited in Figure 11(b). From Figure 11, one can summarize that the ANTSM + MESO algorithm can better control the motor operation at a wide range of speed.

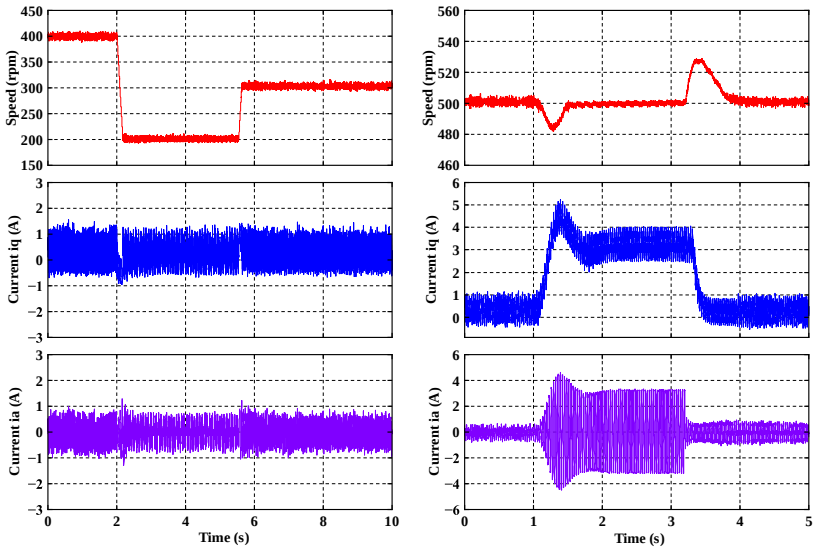

Figure 11. Response curves of ANTSM + MESO controller in low speed region.

5. Conclusions

In this paper, a novel MESO-based ANTSM controller was constructed to improve the anti-disturbance performance of the PMSM drive system with parameter variation and unknown disturbance. To prevent the unsatisfactory control effect due to overestimating switching gain, an adaptive law was combined with the traditional NTSM strategy to achieve the expected performance. Furthermore, compensating the disturbance estimation value obtained by MESO to the ANTSM controller, the switching gain can be further reduced. Comprehensive experimental results demonstrate that the property of the MESO-based ANTSM algorithm outperforms both traditional PI and NTSM control methods. In future work, we will work on solving the stability problem caused by parameter variations.

Use of AI tools declaration

The authors declare they have not used Artificial Intelligence (AI) tools in the creation of this article.

Acknowledgments

This paper was funded by the Natural Science Foundation of the Jiangsu Higher Education Institutions of China under grant number 21KJB510019, the National Natural Science Foundation of China under Grant 62203188, the Natural Science Foundation of Jiangsu Province under Grant BK20220517 and the China Postdoctoral Science Foundation under Grant 2022M721386.

Conflict of interest

The authors declare there is no conflict of interest.

References

1. X. Chen, R. Chen, T. Deng, An investigation on lateral and torsional coupled vibrations of high power density PMSM rotor caused by electromagnetic excitation, *Nonlinear Dyn.*, **99** (2020), 1975–1988. https://doi.org/10.1007/s11071-019-05436-1
2. T. Zhao, S. Wu, S. Cui, Multiphase PMSM with asymmetric windings for more electric aircraft, *IEEE Trans. Transport. Electrific.*, **6** (2020), 1592–1602. https://doi.org/10.1109/TTE.2020.2997609
3. B. Xu, L. Zhang, W. Ji, Improved non-singular fast terminal sliding mode control with disturbance observer for PMSM drives, *IEEE Trans. Transport. Electrific.*, **7** (2021), 2753–2762. https://doi.org/10.1109/TTE.2021.3083925
4. X. Li, D. W. C. Ho, J. Cao, Finite-time stability and settling-time estimation of nonlinear impulsive systems, *Automatica*, **99** (2019), 361–368. https://doi.org/10.1016/j.automatica.2018.10.024
5. X. Li, S. Song, J. Wu, Exponential stability of nonlinear systems with delayed impulses and applications, *IEEE Trans. Autom. Control*, **64** (2019), 4024–4034. https://doi.org/10.1109/TAC.2019.2905271
6. Q. Xie, C. Mu, G. Wu, Z. Yu, R. Jia, Method for flux linkage optimization of permanent magnet synchronous motor based on nonlinear dynamic analysis, *Nonlinear Dyn.*, **97** (2019), 2068–2089. https://doi.org/10.1007/s11071-019-05104-4
7. X. Li, D. Peng, J. Cao, Lyapunov stability for impulsive systems via event-triggered impulsive control, *IEEE Trans. Autom. Control*, **65** (2020) 4908–4913. https://doi.org/10.1109/TAC.2020.2964558
8. F. Wang, H. Xie, Q. Chen, S. Davari, J. Rodriguez, R. M. Kennel, Parallel predictive torque control for induction machines without weighting factors, *IEEE Trans. Power Electron.*, **35** (2020), 1779–1788. https://doi.org/10.1109/TPEL.2019.2922312
9. F. Wang, S. Li, X. Mei, W. Xie, J. Rodrguez, R. M. Kennel, Model-based predictive direct control strategies for electrical drives: an experimental evaluation of PTC and PCC methods, *IEEE Trans. Ind. Informat.*, **11** (2015), 671–681. https://doi.org/10.1109/TII.2015.2423154
10. L. Shanmugam, Y. H. Joo, Design of interval type-2 fuzzy-based sampled-data controller for nonlinear systems using novel fuzzy lyapunov functional and its application to PMSM, *IEEE Trans. Syst. Man Cybern. Syst.*, **51** (2021), 542–551. https://doi.org/10.1109/TSMC.2018.2875098
11. R. Vadivel, Y. H. Joo, Reliable fuzzy H_∞ control for permanent magnet synchronous motor against stochastic actuator faults, *IEEE Trans. Syst., Man, Cybern., Syst.*, **51** (2021), 2232–2245. https://doi.org/10.1109/TSMC.2019.2957001

12. L. Ma, K. Mei, S. Ding, T. Pan, Design of adaptive fuzzy fixed-time HOSM controller subject to asymmetric output constraints, *IEEE Trans. Fuzzy Syst.*, **2023** (2023). https://doi.org/10.1109/TFUZZ.2023.3241147

13. S. Ding, B. Zhang, K. Mei, J. H. Park, Adaptive fuzzy SOSM controller design with output constraints, *IEEE Trans. Fuzzy Syst.*, **30** (2022), 2300–2311. https://doi.org/10.1109/TFUZZ.2021.3079506

14. A. T. Woldegiorgis, X. Ge, H. Wang, M. Hassan, A new frequency adaptive second-order disturbance observer for sensorless vector control of interior permanent magnet synchronous motor, *IEEE Trans. Ind. Electron.*, **68** (2021), 11847–11857. https://doi.org/10.1109/TIE.2020.3047065

15. K. Mei, S. Ding, C.-C. Chen, Fixed-time stabilization for a class of output-constrained nonlinear systems, *IEEE Trans. Syst., Man, Cybern. Syst.*, **52** (2022), 6498–6510. https://doi.org/10.1109/TSMC.2022.3146011

16. X. Jin, Y. Shi, Y. Tang, H. Werner, J. Kurths, Event-triggered fixed-time attitude consensus with fixed and switching topologies, *IEEE Trans. Autom. Control*, **67** (2022), 4138–4145. https://doi.org/10.1109/TAC.2021.3108514

17. K. Chen, W. He, Q. Han, M. Xue, Y. Tang, Leader selection in networks with switching topologies and antagonistic interactions, *Automatica*, **142** (2022), 110334. https://doi.org/10.1016/j.automatica.2022.110334

18. L. Ma, C. Cheng, J. Guo, B. Shi, S. Ding, K. Mei, Direct yaw-moment control of electric vehicles based on adaptive sliding mode, *Math. Biosci. Eng.*, **20** (2023), 13334–13355. https://doi.org/10.3934/mbe.2023594

19. Q. Hou, S. Ding, X. Yu, K. Mei, A super-twisting-like fractional controller for SPMSM drive system, *IEEE Trans. Ind. Electron.*, **69** (2022), 9376–9384. https://doi.org/10.1109/TIE.2021.3116585

20. S. Ding, Q. Hou, H. Wang, Disturbance-observer-based second-order sliding mode controller for speed control of PMSM drives, *IEEE Trans. Energy Convers.*, **38** (2023), 100–110. https://doi.org/10.1109/TEC.2022.3188630

21. W. Dou, S. Ding, X. Yu, Event-triggered second-order sliding mode control of uncertain nonlinear systems, *IEEE Trans. Syst. Man Cybern. Syst.*, **2023** (2023). https://doi.org/10.1109/TSMC.2023.3296681

22. Q. Hou, S. Ding, GPIO based super-twisting sliding mode control for PMSM, *IEEE Trans. Circuits Syst. II Exp. Briefs*, **68** (2021), 747–751. https://doi.org/10.1109/TCSII.2020.3008188

23. K. Mei, S. Ding, Second-order sliding mode controller design subject to an upper-triangular structure, *IEEE Trans. Syst. Man, Cybern. Syst.*, **51** (2021), 497–507. https://doi.org/10.1109/TSMC.2018.2875267

24. Y. Jiang, W. Xu, C. Mu, Y. Liu, Improved deadbeat predictive current control combined sliding mode strategy for PMSM drive system, *IEEE Trans. Veh. Technol.*, **67** (2018), 251–263. https://doi.org/10.1109/TVT.2017.2752778

25. E. Lu, W. Li, X. Yang, Y. Liu, Anti-disturbance speed control of low-speed high-torque PMSM based on second-order non-singular terminal sliding mode load observer, *ISA Trans.*, **88** (2019), 142–152. https://doi.org/10.1016/j.isatra.2018.11.028
26. M. Lv, Y. Li, W. Pan, S. Baldi, Finite-time fuzzy adaptive constrained tracking control for hypersonic flight vehicles with singularity-free switching, *IEEE/ASME Trans. Mechatronics*, **27** (2022), 1594–1605. https://doi.org/10.1109/TMECH.2021.3090509
27. S. Li, M. Zhuo, X. Yu, Design and implementation of terminal sliding mode control method for PMSM speed regulation system, *IEEE Trans. Ind. Informat.*, **9** (2013), 1879–1891. https://doi.org/10.1109/TII.2012.2226896
28. H. Dong, X. Yang, H. Gao, X. Yu, Practical terminal sliding-mode control and its applications in servo systems, *IEEE Trans. Ind. Electron.*, **70** (2023), 752–761. https://doi.org/10.1109/TIE.2022.3152018
29. S. Hou, C. Wang, Y. Chu, J. Fei, Neural network-based adaptive fractional-order terminal sliding mode control, *Trans. Inst. Meas. Control*, **44** (2022), 3107–3117. https://doi.org/10.1177/01423312221098486
30. J. C. Zhang, H. Wang, Z. H. Man, J. Jin, M. Y. Fu, Robust motion control of a linear motor positioner using fast nonsingular terminal sliding mode, *IEEE/ASME Trans. Mechatron.*, **20** (2015), 1743–1752. https://doi.org/10.1109/TMECH.2014.2352647
31. A. K. Junejo, W. Xu, C. Mu, M. M. Ismail, Y. Liu, Adaptive speed control of PMSM drive system based a new sliding-mode reaching law, *IEEE Trans. Power Electron.*, **35** (2020), 12110–12121. https://doi.org/10.1109/TPEL.2020.2986893
32. S. Ding, W. H. Chen, K. Mei, D. J. Murray-Smith, Disturbance observer design for nonlinear systems represented by input-output models, *IEEE Trans. Ind. Electron.*, **67** (2020), 1222–1232. https://doi.org/10.1109/TIE.2019.2898585
33. K. Mei, C. Qian, S. Ding, Design of adaptive SOSM controller subject to disturbances with unknown magnitudes, *IEEE Trans. Circuits Syst. I, Reg. Papers*, **70** (2023), 2133–2142. https://doi.org/10.1109/TCSI.2023.3241291
34. K. Mei, S. Ding, X. Yu, A generalized supertwisting algorithm, *IEEE Trans. Cybern.*, **53** (2023), 3951–3960. https://doi.org/10.1109/TCYB.2022.3188877
35. Y. A. I. Mohamed, Design and implementation of a robust current-control scheme for a PMSM vector drive with a simple adaptive disturbance observer, *IEEE Trans. Ind. Electron.*, **54** (2007), 1981–1988. https://doi.org/10.1109/TIE.2007.895074
36. Y. Zuo, X. Zhu, L. Quan, C. Zhang, Y. Du, Z. Xiang, Active disturbance rejection controller for speed control of electrical drives using phase-locking loop observer, *IEEE Trans. Ind. Electron.*, **66** (2019), 1748–1759. https://doi.org/10.1109/TIE.2018.2838067
37. W. Xu, A. K. Junejo, Y. Liu, M. R. Islam, Improved continuous fast terminal sliding mode control with extended state observer for speed regulation of PMSM drive system, *IEEE Trans. Veh. Technol.*, **68** (2019), 10465–10476. https://doi.org/10.1109/TVT.2019.2926316

38. F. Wang, D. Ke, X. Yu, D. Huang, Enhanced predictive model based deadbeat control for PMSM drives using exponential extended state observer, *IEEE Trans. Ind. Electron.*, **69** (2022), 2357–2369. https://doi.org/10.1109/TIE.2021.3065622
39. K. Yu, Z. Wang, W. Hua, M. Cheng, Robust cascaded deadbeat predictive control for dual three-phase variable-flux PMSM considering intrinsic delay in speed loop, *IEEE Trans. Ind. Electron.*, **69** (2022), 12107–12118. https://doi.org/10.1109/TIE.2022.3142400
40. Z. Liu, D. Yang, Y. Wang, M. Lu, R. Li, EGNN: Graph structure learning based on evolutionary computation helps more in graph neural networks, *Appl. Soft Comput.*, **135** (2023), 110040. https://doi.org/10.1016/j.asoc.2023.110040
41. Y. Wang, Z. Liu, J. Xu, W. Yan, Heterogeneous network representation learning approach for Ethereum identity identification, *IEEE Trans. Comput. Social Syst.*, **10** (2023), 890–899. https://doi.org/10.1109/TCSS.2022.3164719
42. Y. Shi, L. Li, J. Yang, Y. Wang, S. Hao, Center-based transfer feature learning with classifier adaptation for surface defect recognition, *Mech. Syst. Signal Process.*, **188** (2023), 110001. https://doi.org/10.1016/j.ymssp.2022.110001
43. Y. Shi, H. Li, X. Fu, R. Luan, Y. Wang, N. Wang, et al., Self-powered difunctional sensors based on sliding contact-electrification and tribovoltaic effects for pneumatic monitoring and controlling, *Nano Energy*, **110** (2023), 108339. https://doi.org/10.1016/j.nanoen.2023.108339
44. C. Tian, Z. Xu, L. Wang, Y. Liu, Arc fault detection using artificial intelligence: Challenges and benefits, *Math. Biosci. Eng.*, **20** (2023), 12404–12432. https://doi.org/10.3934/mbe.2023552
45. Q. K. Hou, S. H. Ding, X. H. Yu, Composite super-twisting sliding mode control design for PMSM speed regulation problem based on a novel disturbance observer, *IEEE Trans. Energy Convers.*, **36** (2021), 2591–2599. https://doi.org/10.1109/TEC.2020.2985054
46. S. Ding, L. Liu, J. H. Park, A novel adaptive nonsingular terminal sliding mode controller design and its application to active front steering system, *Int. J. Robust Nonlinear Control*, **29** (2019), 4250–4269. https://doi.org/10.1002/rnc.4625
47. J. Yang, T. Li, C. Liu, S. Li, W. H. Chen, Nonlinearity estimator-based control of a class of uncertain nonlinear systems, *IEEE Trans. Autom. Control*, **65** (2020), 2230–2236. https://doi.org/10.1109/TAC.2019.2940567
48. Y. Feng, X. Yu, Z. Man, Non-singular terminal sliding mode control of rigid manipulators, *Automatica*, **38** (2002), 2159–2167. https://doi.org/10.1016/S0005-1098(02)00147-4
49. A. Levant, Principles of 2-sliding mode design, *Automatica*, **43** (2007), 576–586. https://doi.org/10.1016/j.automatica.2006.10.008
50. S. Yu, X. Yu, B. Shirinzadeh, Z. Man, Continuous finite-time control for robotic manipulators with terminal sliding mode, *Automatica*, **41** (2005), 1957–1964. https://doi.org/10.1016/j.automatica.2005.07.001